Early Hepatic Lesions Display Immature Tertiary Lymphoid Structures and Show Elevated Expression of Immune Inhibitory and Immunosuppressive Molecules

Maxime Meylan[1,2], Florent Petitprez[1,2], Laetitia Lacroix[1], Luca Di Tommaso[3,4], Massimo Roncalli[3,4], Antoine Bougoüin[1], Alexis Laurent[5], Giuliana Amaddeo[6,7], Daniele Sommacale[5,7], Hélène Regnault[6], Jonathan Derman[8], Cécile Charpy[8], Fouad Lafdil[7], Jean-Michel Pawlotsky[7,9], Catherine Sautès-Fridman[1], Wolf H. Fridman[1], and Julien Calderaro[1,7,8]

ABSTRACT

Purpose: The impact of tertiary lymphoid structures (TLS) in hepatocellular carcinoma (HCC) progression is being extensively investigated. However, their presence during the early steps of human liver carcinogenesis remains unknown. We thus aimed to determine whether TLS are induced in preneoplastic/early hepatic lesions (EHL), and whether they are associated with a particular immune profile.

Experimental Design: A series of 127 EHLs (low/high-grade dysplastic nodules, early HCC, and small and progressed HCC) was included in the study. TLSs were investigated by pathologic reviewing. Densities of immune cells were assessed using IHC. A subset of lesions was microdissected and gene expression profiling was performed with a custom NanoString panel.

Results: Compared with surrounding cirrhotic nodules, EHL of all stages displayed increased densities of T cells, B cells, and dendritic cells. Immature TLSs were identified in 24% of EHL. Gene expression profiling identified a subset of EHL with elevated mRNA levels of various cytokines involved in immune cells' recruitment and TLS induction. This subgroup of EHL also showed overexpression of genes related to T- and B-cells' activation and antigen presentation, as well as those related to immunosuppression and immune exhaustion.

Conclusions: Local immune activation occurs in the very early steps of liver carcinogenesis; however, it may not be fully efficient and paradoxically favor immune evasion and progression to full-blown HCC. These results have implications for the development of anti-HCC chemopreventive strategies in cirrhotic patients.

Introduction

Hepatocellular carcinoma (HCC), the most frequent primary liver cancer, is the fourth leading cause of cancer-related death worldwide (https://gco.iarc.fr/). Its risk factors comprise chronic alcohol intake, infection by hepatitis B (HBV) or hepatitis C (HCV) viruses, nonalcoholic steatohepatitis (NASH), and rare genetic diseases (1). These factors lead to chronic liver inflammation and tissue damage, and, in Western countries, more than 90% of HCC are diagnosed in cirrhotic patients (1). A better understanding of the biological mechanisms that link chronic liver injury to malignant transformation is mandatory to improve early diagnosis and/or to propose preventive treatments. Carcinogenesis on cirrhotic livers is a multistep process, and, based on histopathologic criteria, a consensus classification describing the different stages of malignant transformation has been proposed and is now widely accepted (2–6). These "early hepatic lesions" (EHL) are classified as low-grade dysplastic nodules (LGDN), high-grade dysplastic nodules (HGDN), early HCC (eHCC), or small and progressed HCC (spHCC; ref. 4).

Several studies performed in animal models support a key role of the inflammatory/immune microenvironment in the early steps of malignant transformation (7–12). Indeed, He and colleagues showed that HCC progenitor cells give rise to full-blown tumors only when introduced into a chronically injured liver, and further demonstrated that transformation relied on several inflammatory/immune mediators including IL6 and TNF (9). Activation of inflammatory pathways, including NF-κB, was also identified as a critical step for the development of tumors that arise in chronically injured organs, such as HCC or colitis-associated colorectal cancer (12, 13).

The role of tertiary lymphoid structures (TLS) in cancer is also drawing an increasing attention (14). They are defined as ectopic lymphoid aggregates located in chronically inflamed tissues, and play a pivotal role in the promotion of *in situ* adaptive immune responses toward locally displayed antigens (14). Their formation is a complex process that relies on several chemokines produced in response to

[1]Centre de Recherche des Cordeliers, INSERM, Sorbonne Université, USPC, Université de Paris, Inflammation, Complement and Cancer Team, Paris, France. [2]Programme Cartes d'Identité des Tumeurs, Ligue Nationale Contre le Cancer, Paris, France. [3]Department of Pathology, Humanitas Clinical and Research Center - IRCCS, Rozzano, Milan, Italy. [4]Department of Biomedical Sciences, Humanitas University, Rozzano, Milan, Italy. [5]Service de Chirurgie Digestive et Hépatobiliaire, Assistance Publique Hôpitaux de Paris, Groupe Hospitalier Henri Mondor, Créteil, France; Université Paris-Est Créteil, Créteil France. [6]Assistance Publique–Hôpitaux de Paris, Service d'Hépatologie, Hôpital Henri Mondor, Paris, France. [7]Inserm U955, Equipe 18, Institut Mondor de Recherche Biomédicale, Créteil, France, Université Paris Est Créteil, Créteil, France. [8]Département de Pathologie, Assistance Publique Hôpitaux de Paris, Groupe Hospitalier Henri Mondor, Créteil, France; Université Paris-Est Créteil, Créteil France. [9]APHP, Groupe Hospitalier Henri Mondor, Service de Virologie, Bactériologie-Hygiène, Mycologie-Parasitologie et unité Transversale de Traitement des Infections, Créteil, France.

Note: Supplementary data for this article are available at Clinical Cancer Research Online (http://clincancerres.aacrjournals.org/).

Corresponding Author: Julien Calderaro, Centre Hospitalier Universitaire Henri-Mondor, 51 Av du Maréchal de Lattre de Tassigny, Créteil 94010, France. Phone: 334-981-2732; Fax: 334-981-2733; E-mail: julien.calderaro@aphp.fr

Clin Cancer Res 2020;26:4381–9

doi: 10.1158/1078-0432.CCR-19-2929

©2020 American Association for Cancer Research.

Downloaded from http://aacrjournals.org/clincancerres/article-pdf/26/16/4381/2062504/4381.pdf by guest on 27 August 2022

Translational Relevance

Our study shows that a significant subset of early hepatic lesions displays formation of tertiary lymphoid structures and immune activation, along with overexpression of cytokines reported to be procarcinogenic in mice. This immune response appears inefficient to prevent progression to full-blown hepatocellular carcinoma, and the expression of various immune checkpoint and immunosuppressive molecules in this subset of lesions may favor immune evasion.

various inflammatory stimuli (14). Pathologic and IHC studies identified several TLS maturation stages (15–17). They are classified as fully mature if their morphologic analysis reveals a clear and central area resembling germinal centers found in secondary lymphoid structures (7, 14–17). We showed in a series of 273 patients that the presence of TLS within the tumor and their degree of maturation were linked with lower rates of early relapse (17). Consistently, we also observed that the aggressive macrotrabecular-massive HCC subtype was associated with a lack of TLS (17–20).

Interestingly, using mice models of HCC induced by chronic NF-κB signaling pathway activation, Finkin and colleagues observed that TLS located in the nontumoral liver could promote the transformation of malignant progenitors through the production of various cytokines, including LTβ, CCL17 and CCL20 (7). Accordingly, they reported, in a cohort of patients with HCC treated by surgical resection, that the presence of TLS in the nontumoral liver was associated with an increased risk for late tumor recurrence and a trend toward decreased overall survival (7).

We aimed in this study to determine, by means of gene expression profiling, IHC, and digital pathology, whether TLS formation occurs in human EHL, and the associations between TLS presence, immune profile, and nodule grade. We show that a significant fraction of EHL display TLS and immune activation, along with overexpression of cytokines demonstrated to be procarcinogenic in mice models. This immunity may not be fully efficient, as EHL lack fully mature TLS and show high expression of immune inhibitory and immunosuppressive molecules.

Materials and Methods

Patients and samples

We retrospectively included patients who underwent liver resection or transplantation at Henri Mondor University Hospital (Créteil, France) between 2005 and 2015. Inclusion criteria were as follows: available histologic slides and formalin-fixed, paraffin-embedded blocks, unequivocal diagnosis of EHL, and lack of prior antitumor therapy. The following clinical features were systematically recorded: age, gender, and risk factors of liver disease (alcohol use disorder, HBV or HCV infection, and NASH). The study was conducted in accordance with the Declaration of Helsinki and approved by an institutional review board. Written informed consent was obtained.

Histologic slides were reviewed independently by three pathologists specialized in liver disease (L. Di Tommaso, M. Roncalli, and J. Calderaro), and EHL were classified as LGDN, HGDN, eHCC, or spHCC, according to previously published criteria (nuclear atypia, unpaired arteries, loss of reticulin framework, pseudoglandular formations, and stromal invasion; ref, 4). Cases with disagreement were discussed and a consensus was reached.

TLS located inside cirrhotic nodules were assessed on hematoxylin-eosin-saffron–stained sections, and they were defined as clusters of immune cells (21). They were further classified as aggregates, primary follicles, or secondary follicles based on their morphologic appearance, as published previously (7, 17, 21).

IHC and immune cells densities

All immunostainings were performed on 3-μm thick whole sections prepared from formalin-fixed, paraffin-embedded blocks. The following primary antibodies were used: CD3 (Ventana CONFIRM, Clone 2GV6, no dilution), CD8 (Dako, Clone C8/1448, dilution: 1/200), CD20 (Dako, Clone L26, dilution: 1/500), DCLamp (Dendritics, 1010.01, dilution: 1/801), Myeloperoxidase (MPO, Dako, A0398, dilution: 1/2,000), CD21 (Leica, Clone 2G9, dilution: 1/50), CD4 (AF-379-NA, dilution: 1/200), PDL1 (Cell Signaling Technology, E1L3N, dilution: 1/100), and CD163 (Leica, Clone 10D6, dilution: 1/400).

CD3/DCLamp double stainings and CD4 stainings were performed manually. After deparaffinization and rehydration, the sections were placed into a target retrieval solution (Agilent, Target Retrieval Solution). Endogenous peroxidase, alkaline phosphatase, and nonspecific background staining were blocked with Endogenous Dual Block (Dako) and Protein Block (Dako) reagents. Detection was further performed using secondary antibodies (Polymer anti-Goat IgG, Goat anti-rabbit IgG, and Biotin Donkey anti-Rat IgG). Peroxidase and alkaline phosphatase activity were revealed using 3-amino-9-ethylcarbazole substrate (Vector Laboratories) and alkaline phosphatase substrate III (Vector Laboratories).

For CD8, CD20, MPO, CD21, PDL1, and CD163 stainings, slides were processed on an automated immunostainer (Leica Bond-Max; Leica Biosystems) according to the manufacturer's instructions. Endogenous peroxidase was blocked using Peroxide Block (Bond Polymer Refine Detection Kit, Leica Biosystems). Antigen retrieval was performed using E1 (pH 6; CD20, CD163, MPO, and CD21) or E2 (pH 9; CD8 and PDL1) reagents. Immunodetection was performed using Polymer and 3,3′ di-aminobenzidine (Bond Polymer Refine Detection Kit, Leica Biosystems).

For CD4, slides were scanned at 40× magnification using a NanoZoomer Device (Hamamatsu). Quantification of immune cells located within the EHL was performed using dedicated software for digital slides analysis (Calopix, Tribun Medical). Densities were expressed as the mean number of positive cells per mm^2. Normalization was performed using the densities of cells located within three adjacent surrounding nodules. For PDL1 staining, we chose to quantify the area of staining, as positive cells, most often arranged in clusters, were difficult to count.

To truly capture what happens strictly within cirrhotic nodules, we only assessed immune cells located within the nodules, and not the ones located in the fibrous areas of cirrhosis.

Laser microdissection and RNA extraction

Ten-micrometer-thick sections were prepared from paraffin-embedded blocks using a microtome and PEN2 Glass Membrane Slides (Leica Microsystems). After a fast toluidine blue staining procedure, sections were air-dried for 5 minutes. EHL and three surrounding nodules for each patient (for normalization) were further microdissected with a Leica Laser Capture Microdissection

Downloaded from http://aacrjournals.org/clincancerres/article-pdf/26/16/4381/2062504/4381.pdf by guest on 27 August 2022

Table 1. Clinical, biological, and pathologic features of the 41 patients and the 127 EHLs.

Clinical features of the patients ($N = 41$)		
Gender	M/F	32 (78%)/9(22%)
Age	Median (range)	61 (45–70)
Risk factors	Alcohol	27 (58%)
	HCV	10 (24%)
	HBV	3 (7%)
	NASH	6 (15%)
	Undetermined	2 (5%)
Surgery	Resection/transplantation	10 (24%)/31 (76%)
Pathologic features of EHLs ($N = 127$)		
Disease stage	Low-grade macronodule	31 (24%)
	High-grade macronodule	17 (13%)
	eHCC	24 (20%)
	spHCC	55 (43%)

System (Leica Biosystems). RNAs were isolated using the RNeasy FFPE Kit (Qiagen) and qualified with a 2100 Bioanalyzer (Agilent).

Gene expression profiling

We used a custom NanoString gene panel that includes 269 genes involved in various immune-related biological pathways such as antigen processing and presentation, immune cell recruitment, and T- and B-cells' activation and function (Supplementary Table S1). Gene expression data normalization was performed with NanoString nSolver version 3.0 software with default parameters. To reduce noise, background thresholding was applied, and probes counts with values lower than the background threshold were substituted by the threshold count value. The threshold was computed as the geometric mean of eight negative spike-in controls. Furthermore, a positive control normalization factor was calculated from the geometric mean of six positive spike-in controls. Probe with counts within the 0.3–3 range were included. Similarly, data were normalized against the geometric mean of 16 housekeeping genes. Probes within the 0.1–10 interval were selected and $\log_2$ transformed.

Statistical analysis

Statistical analysis was performed using the R software version 3.6.0 and the packages pheatmap and ggplot2 (22). The relationship between categorical and quantitative variables was estimated with the Mann–Whitney U test (two categories) or the Kruskal–Wallis test (three or more categories). Associations between categorical variables were estimated by Fisher exact test. When appropriate, P values were corrected for multiple hypothesis testing with the Benjamini–Hochberg method. $P < 0.05$ was considered for significance.

Results

Patients and samples

Patients were mostly males (32/41, 78%) and all had established cirrhosis (**Table 1**). Median age at surgery was 61 years. Risk factors of chronic liver disease were alcohol use disorder (27/41, 58%), hepatitis

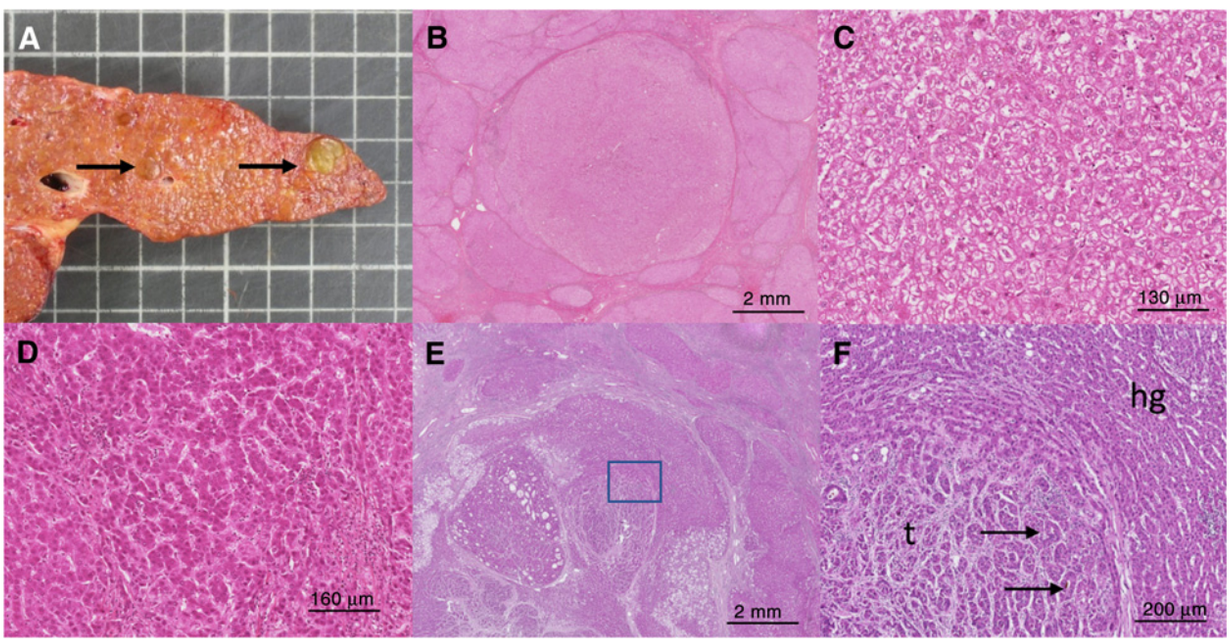

Figure 1.

Macroscopic and microscopic features of EHLs. **A,** Gross examination of this cirrhotic liver shows several atypical nodules corresponding to EHLs (black arrows). **B,** Low magnification of an EHL: the nodule is well demarcated from the surrounding cirrhotic parenchyma (hematoxylin-eosin-saffron, HES). **C,** Microscopic examination of LGDN does not show any significant cellular atypia (HES). This spHCC shows large areas of malignant transformation (HES). **D,** A high grade EHL with increased cellular density. **F,** High magnification of the area framed in **E**: the high-grade area shows increased cellular density and thick trabeculae (hg). Examination of the transformed area (t) reveals pseudoglandular formations (black arrows; HES).

Downloaded from http://aacrjournals.org/clincancerres/article-pdf/26/16/4381/2062504/4381.pdf by guest on 27 August 2022

C (10/41, 24%), NASH (6/41, 15%), and HBV (3/41, 7%; **Table 1**). Mixed etiologies were identified in 9 patients. Thirty-one patients were treated by liver transplantation and 10 by liver resection. The number of EHL sampled per patient varied from 1 to 7.

According to histologic criteria recognized by the International Working Party, consensus pathologic reviewing identified a total of 31 LGDNs (24%), 17 HGDNs (13%), 24 eHCCs (20%), and 55 spHCCs (43%; **Fig. 1**). Median diameter of the EHL was 10 mm (no differences were observed according to EHL stage).

EHL immune infiltrates differ from those of surrounding nodules

EHL were characterized by overall higher densities of immune cells than their corresponding surrounding nodules (**Fig. 2A**; Supplementary Fig. S1). Average densities of $CD3^+$, $CD4^+$ T cells, and $CD20^+$ B cells were increased by 3-fold (CD4 was performed in 56 cases with material available). While significant, smaller differences were observed for $CD8^+$ lymphocytes, $DCLamp^+$ dendritic cells, $CD163^+$ macrophages, and MPO^+ neutrophils with fold

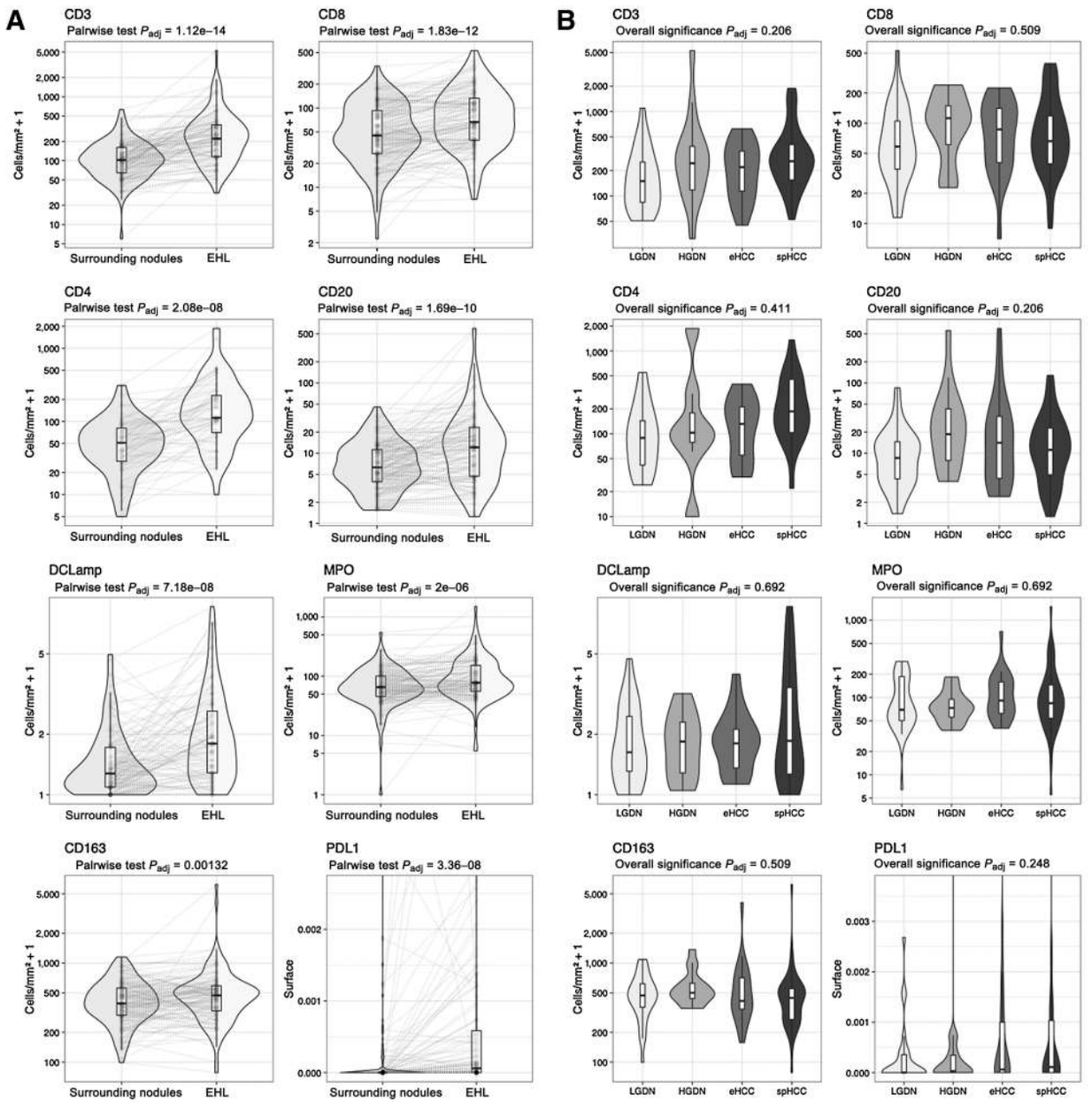

Figure 2.

Densities of immune cells infiltrating EHL. **A,** Pairwise comparisons of the immune infiltrates between EHL and their respective surround nodules. Violin plots containing boxplots highlighting the median; the strings identify each EHL linked to their surrounding nodules. **B,** Immune cell densities across EHL histologic grades. Violin plots containing boxplots highlighting the median.

Downloaded from http://aacrjournals.org/clincancerres/article-pdf/26/16/4381/2062504/4381.pdf by guest on 27 August 2022

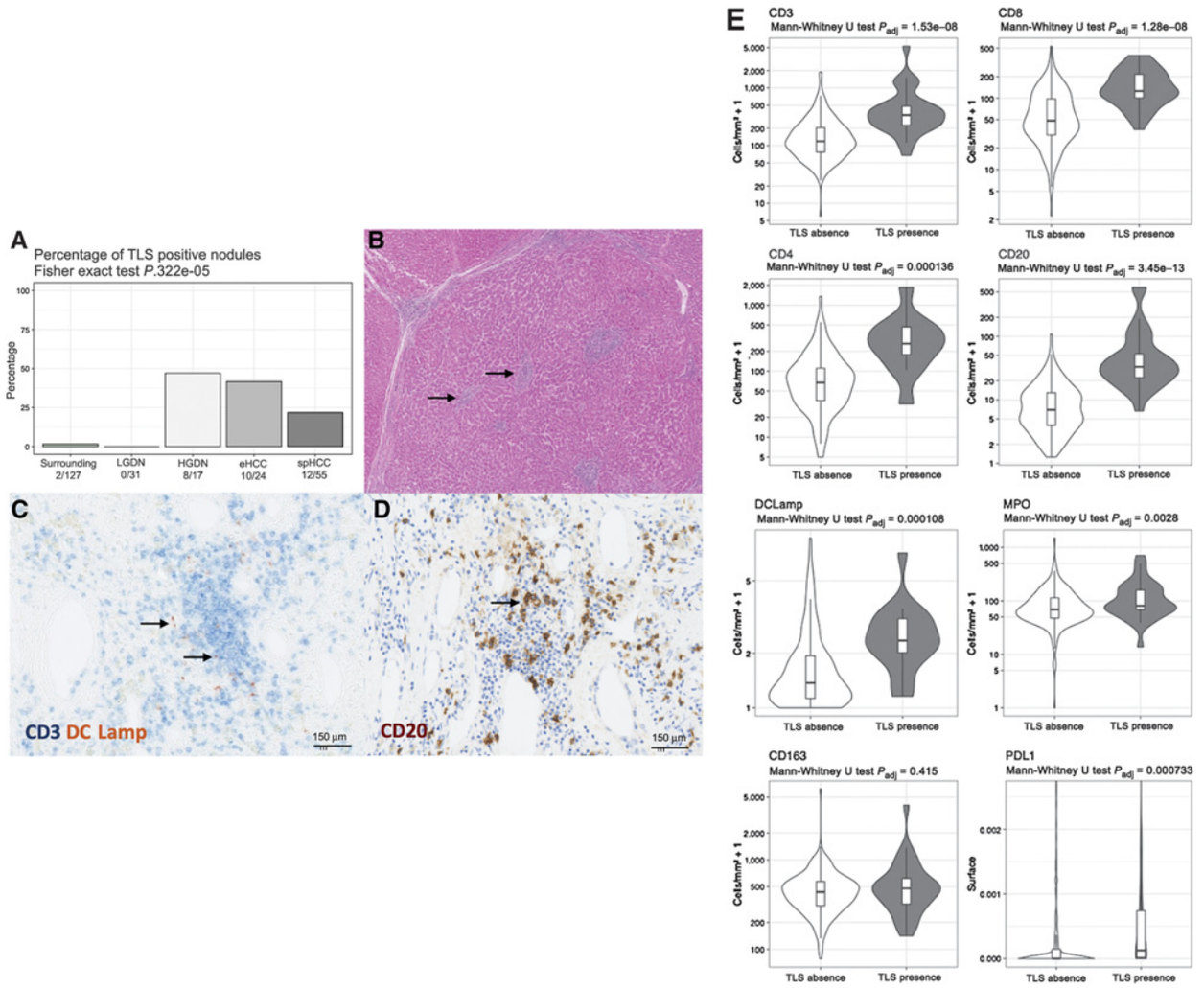

Figure 3.

Identification of TLSs in EHL. **A,** Pathologic reviewing identified TLS in HGDN (47%), eHCC (42%), and spHCC (22%). **B,** This eHCC features numerous TLS [black arrows, hematoxylin-eosin-saffron (HES)]. **C,** IHC staining of a TLS; numerous DCLamp$^+$ dendritic cells were identified (black arrows, red staining) in the vicinity of a T-cell aggregate (CD3 staining; blue). **D,** The TLS depicted in **C** also includes CD20$^+$ B cells. **E,** EHL bearing morphologic TLS show higher densities of T cells, B cells, and DCLamp dendritic cells.

changes ranging from 1.27 to 1.53 (**Fig. 2A**; Supplementary Fig. S1). Interestingly, we also identified higher areas of PDL1 staining in EHL compared with matched surrounding nodules (**Fig. 2A**).

We further compared the immune cell densities according to EHL stage and, after adjustment for multiple testing, no statistical differences were evidenced. However, although distribution of CD20$^+$ B-cell densities was heterogeneous among HGDN samples, a 4-fold mean increase was evidenced between LGDN and HGDN (**Fig. 2B**). No other differences were observed between the different grades for the other cell populations (**Fig. 2B**).

Finally, we investigated whether the variations of immune cells' densities between EHL and their respective surrounding nodules differed according to etiologies of liver disease. We did not find any statistically significant changes between the etiologies of liver disease (data not shown).

Pathologic detection of TLS in EHL

By pathologic reviewing, we searched for the presence of TLS in the whole series of 127 EHL and their matched surrounding nodules. TLSs were detected in 30 of 127 lesions (**Fig. 3A** and **B**). These 30 lesions were identified in a total of 18 different patients. While no TLSs were observed in LGDN, they were identified in 47% and 42% of HGDN and eHCC, respectively. The frequency of TLS detection was lower for spHCC (21%; **Fig. 3A**). IHC stainings confirmed that TLS included T cells, B cells, and DCLamp$^+$ dendritic cells (**Fig. 3C** and **D**). All, but one, TLSs identified within the EHL were classified as aggregates, with the remaining one being a primary follicle. No secondary follicle was detected. Strikingly, we found TLS in only two cases of surrounding nodules (2/127; **Fig. 3A**). No association between nodule diameter and TLS presence was observed. We finally assessed whether the presence of TLS in EHL was associated to their presence in adjacent, full-blown HCC. Thirty-one patients underwent surgery for HCC, and TLSs were

Downloaded from http://aacrjournals.org/clincancerres/article-pdf/26/16/4381/2062504/4381.pdf by guest on 27 August 2022

present in 39% of the tumor samples. In addition, patients with TLS-positive adjacent HCC were more likely to have TLS-positive EHL ($P = 0.007$), we found 41% of TLS-positive EHL when the adjacent HCC contained TLS, and only 15% TLS-positive EHL when the adjacent HCC was TLS negative (Supplementary Fig. S2)

TLS-positive EHL displayed higher densities of total $CD3^+$, $CD8^+$, $CD4^+$ T lymphocytes, $CD20^+$ B cells, and $DCLamp^+$ mature dendritic cells, as well as higher PDL1 labeling than EHL without detectable TLS (**Fig. 3E**). Only weak or no statistical differences were observed for MPO^+ neutrophils ($P_{adj} = 0.028$) and $CD163^+$ macrophages ($P_{adj} = 0.415$). In-line with their immature morphologic appearance, most TLS in EHL (91%, 19/21 cases with material available) lacked $CD21^+$ follicular dendritic cells (Supplementary Fig. S1). We then searched for associations between TLS and liver disease etiologies. Alcohol use disorder and HBV infection were associated with lower and higher frequencies of TLS located within EHL ($P_{adj} = 0.0259$ and $P_{adj} = 0.00195$, respectively; Supplementary Fig. S3A). This finding may however be due to an enrichment in grades with low TLS frequency (LGDN and spHCC; $P_{adj} = 0.0673$) for patients with alcohol use disorder and in grades with high TLS frequency (HGDN and eHCC; $P_{adj} = 0.0184$) for patients with HBV infection (Supplementary Fig. S3B). TLSs induced during HCV infection were located within fibrous bands or portal tracts, and we did not identify increased numbers of TLS in HCV-associated EHL as our study focused on the intranodular immune microenvironment. Finally, we performed an unsupervised clustering of the immune cell densities of the EHL (Supplementary Fig. S3C). While lesions from the same patient tended to group together, TLS presence was associated with an immune-rich cluster (highlighted in red, Supplementary Fig. S3C). Etiologies and EHL grade did not seem to be associated with a particular immune profile.

Identification of an immune-high subtype of EHL, based on gene expression profiling

To further characterize the immune modulations that occur during malignant transformation, we micro-dissected a series of 32 randomly selected EHL developed in 15 patients. These EHLs were graded as LGDN (6/32), HGDN (5/32), eHCC (8/32), and spHCC (13/32). For each case, three nonspecific surrounding cirrhotic nodules from the same liver were also dissected for data normalization. This approach allowed us to limit potential biases related to the underlying liver disease.

On the basis of our previous phenotypical findings, we first assessed a gene expression signature related to TLS induction and formation that has been validated in various cancers including HCC (7, 17, 23, 24). This signature has also been validated in cirrhotic, nontumoral liver tissues and comprises 12 chemokines involved in immune cells recruitment and activation (7).

For each EHL, the geometric mean expression of the 12 genes was calculated and two groups, 12 chemokines high (12-$chem^{hi}$) and 12 chemokines low (12-$Chem^{lo}$), were defined (the median was used as the cut-off value). Noticeably, of the nine cases with morphologic TLS identified on hematoxylin-eosin-saffron–stained sections, eight belonged to the 12-$chem^{hi}$ group, a finding that further validates the use of the signature (**Fig. 4A**).

12-$chem^{hi}$ EHL display higher densities of infiltrating immune cells and a gene expression profile suggestive of an ongoing immune response

We assessed the densities of infiltrating immune cells in EHL according to the expression of the 12-chemokines signature (**Fig. 4B**). We compared the two subgroups of EHL and found increased densities of $CD3^+$, $CD4^+$ ($P_{trend} = 0.1$, staining was only available in 19 cases), $CD8^+$ and $CD20^+$ lymphocytes, and $DCLamp^+$ dendritic cells, as well as higher PDL1 labeling, in 12-$chem^{hi}$ EHL compared with 12-$chem^{lo}$ EHL (**Fig. 4B**), in accordance with the variation of cell densities associated to the presence of morphologic TLS (**Fig. 3E**).

Using our custom NanoString panel, we further analyzed the expression of 269 genes involved in various immunologic processes and identified 89 genes differentially expressed between the 12-$chem^{hi}$ and 12-$chem^{lo}$ EHL (**Fig. 4C**). Consistent with the induction of TLS, the 12-$chem^{hi}$ group showed higher expression of lymphotoxin-alpha (LTA) and lymphotoxin-beta (LTB), two cytokines involved in the development of secondary lymphoid organs and TLS [fold change of 2.5 ($P_{adj} = 0.02$) and 2.0 ($P_{adj} = 0.02$), respectively; Supplementary Table S2].

Increased levels of genes related to key TLS immune cell subsets were also observed: *CD2, CD3D*, and *TRAT1* (T cells), *BANK1, CD79A, CD79B, MS4A1, IGHA1*, and *IGHD* (B cells), *CLIC2, CLEC4C, CLEC7A, CLEC10A, WFDC21P*, and *CD1E* (dendritic cells), and *VEGFB, CDH5*, and *VWF* (endothelial cells; **Fig. 4C**; Supplementary Table S3).

We further identified higher expression of genes related to T-cell activation and function (*CD80, CD40LG, IL2RA, IL2RG, ICOS, ZAP70*, and *CD27*), cytotoxicity (*PRF1*), and promotion of antigen presentation (*HLA-A, HLA-C*, and *B2M*) in this subgroup of lesions, supporting the existence of an *in situ* immune response (**Fig. 4C**).

Interestingly, we also detected an overexpression of several immunosuppressive molecules (*IL10RA, TGFB1*, and *LILRB2*) and immune exhaustion markers (*HAVCR2* and *PDCD1LG2*, respectively, encoding Tim-3 and PD-L2) in the 12-$chem^{hi}$ subgroup. Results for *IL10RB* ($P = 0.054$), *PDCD1* ($P = 0.12$), and *CTLA-4* ($P = 0.095$) were also close to significance (Supplementary Table S2). Finally, expression levels of several proinflammatory cytokines including *IL1B, IL32*, and *IL6* were also characteristic of the 12-$chem^{hi}$ subgroup.

Discussion

Immune modulations have been extensively investigated in full-blown HCC and animal models of liver carcinogenesis (19, 20, 25–27); however, their involvement in human preneoplastic lesions remained to be determined. Although the study of antitumor immunity in cirrhotic patients is often considered challenging due to the underlying liver disease, our approach, which includes normalization according to surrounding nodules and focus on the changes occurring strictly within the nodules, allowed us to limit this potential bias.

We identified increased densities of immune cell populations, including T and B cells, mature dendritic cells, macrophages, and neutrophils in EHL compared with surrounding cirrhotic nodules. Immature TLS were also identified in HGDN, eHCC, and spHCC but not in LGDN.

Expression of a TLS selective 12-chemokines gene signature provided further evidence that TLSs are induced in EHL. Quantification of cell densities confirmed that 12-$chem^{hi}$ EHL display higher densities of various immune cell populations, including $CD4^+$, $CD8^+$ T cells, $CD20^+$ B cells, and $DCLamp^+$ dendritic cells, as well as higher PDL1 labeling.

None of the 127 cases included in our study featured any morphologically mature TLS and only one displayed a primary follicle. In-line with this immature appearance, most TLS-positive EHL lacked $CD21^+$ follicular dendritic cells.

Downloaded from http://aacrjournals.org/clincancerres/article-pdf/26/16/4381/2062504/4381.pdf by guest on 27 August 2022

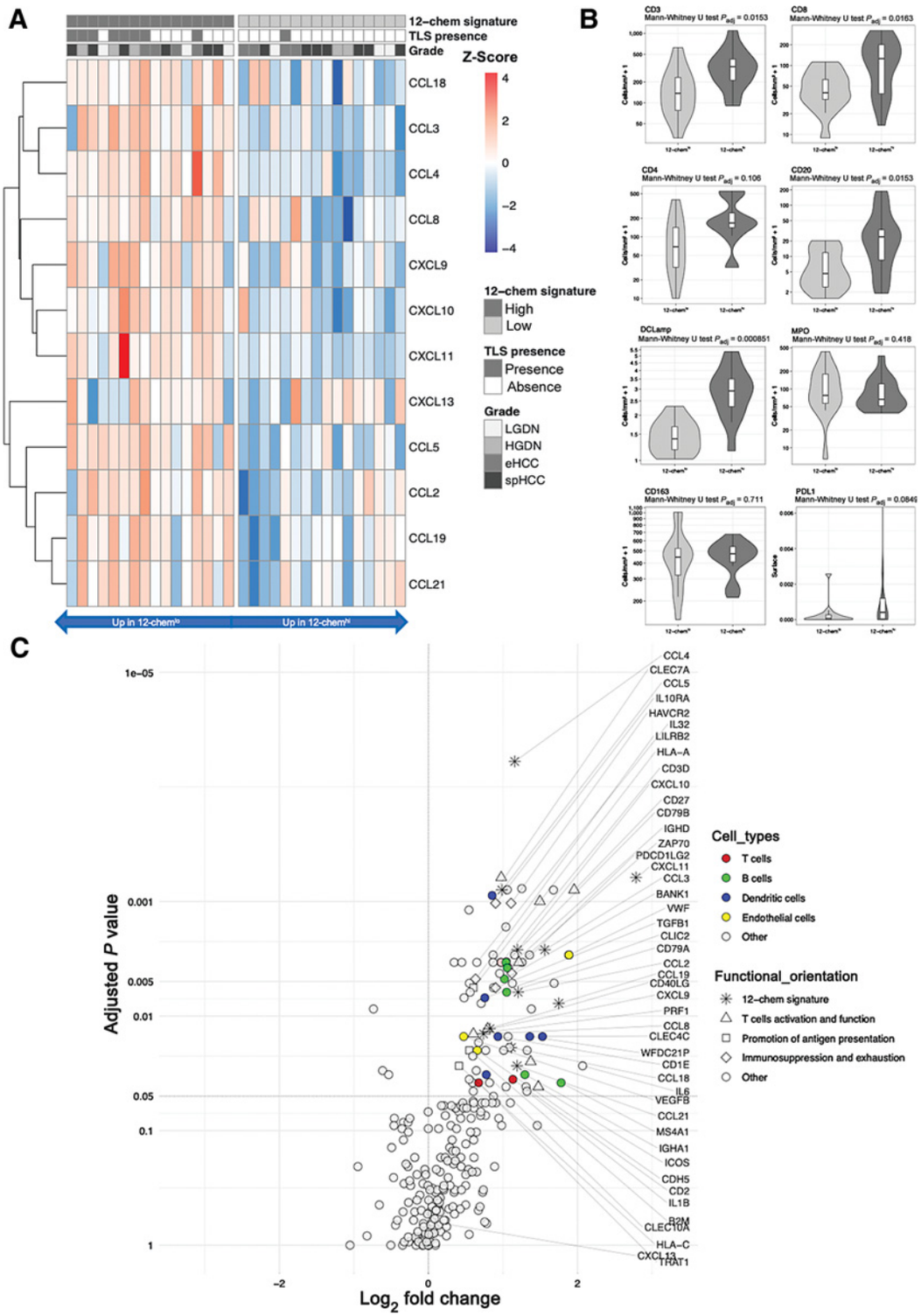

Figure 4.

Characterization of 12-chemokines high and low group. **A,** Heatmap presenting normalized gene expression of the 12-chemokines signature. The 12-chemokine group on the left displayed a higher mean expression of the 12 genes than the 12-chemokine group on the right. **B,** Immune cell densities according to the expression of the 12-chemokine gene signature. Violin plots containing boxplots highlighting the median. **C,** Volcano plots representing differentially expressed genes between the 12-Chem^{hi} and the 12-Chem^{lo} groups within the 269 genes of the custom NanoString panel. Colors indicate genes representative of cell types; shapes show functional orientation of illustrated genes.

Downloaded from http://aacrjournals.org/clincancerres/article-pdf/26/16/4381/2062504/4381.pdf by guest on 27 August 2022

A subset of 12-chem^{hi} EHL did not feature TLS on hematoxylin and eosin–stained sections, and we may hypothesize that in these cases TLSs were still in the process of being formed and were thus not yet morphologically identifiable. This may however also be related to sampling heterogeneity.

EHL classified as 12-chem^{hi} were characterized by the expression of a large array of immune genes. Several hallmarks of immune responses were shown to be activated, such as MHC class I expression or T- and B-cell activation and proliferation. Expression of perforin, an effector molecule necessary for CD8 and natural killer cell cytotoxicity, was also upregulated in these samples. Further studies are needed to determine the main drivers of these immune responses that occur in the very first steps of carcinogenesis (e.g., genetic and/or epigenetic alterations, global deregulations in gene expression etc.).

Although the presence of TLS and the set of genes overexpressed are suggestive of a local activation of immunity, we acknowledge that we cannot conclude on the impact of this response on the progression of TLS-positive EHL. Frequency of TLS was lower in spHCC than HGDN and eHCC, and this finding may either reflect the regression of a subset of TLS-positive HGDN/eHCC or the development of particular immunosuppressive mechanisms in spHCC. Sequential biopsy samples of EHL would be necessary to assess their evolution over time (regression or development into full-blown HCC?). Such samples are, however, impossible to obtain due to ethical and/or practical issues and the fate of these immune-activated lesions remains to be determined.

Several findings suggest that this *in situ* immune activation may not be fully efficient.

First, in 12-chem^{hi} EHL we identified increased mRNA levels of *PDCD1LG2*, which encodes PD-L2, and *HAVCR2*, which encodes Tim-3. Although not increased at the mRNA level in 12-chem^{hi} EHL, PDL1 expression was also increased in EHL compared with their corresponding surrounding nodules, and it was higher in TLS-positive EHL. These different molecules have the ability to negatively regulate T-cell responses and are considered some of the most potent inhibitors of immune responses (28). The second line of evidence is that the 12-chem^{hi} subset exhibited high expression of genes encoding several immunosuppressive molecules such as IL10, TGFβ, and LILRB2. Finally, no mature TLS and only one primary follicle were detected in EHL, the vast majority of the lesions harboring only lymphocytic aggregates. This type of lymphoid structures may indeed not be able to fully promote B-cell activation, proliferation, and differentiation. We, however, acknowledge that we cannot firmly conclude on the functionality of this response. Other approaches, such as T-cell receptor or B-cell receptor sequencing, may noticeably help to determine whether clonal/oligoclonal immune cells are induced.

Immunity has been shown to play an ambiguous role in liver carcinogenesis, and some of the gene expression modulations observed may also paradoxically promote tumor growth. Several key inflammatory or immune mediators overexpressed in 12-chem^{hi} EHL, such as *IL6* or *LTB*, had indeed been reported, in animal models, to promote malignant transformation (9, 29). Using murine models of NASH, Shalapour and colleagues showed that immunoglobulin-A (IgA) producing cells suppress antitumor cytotoxic responses (30). Consistently, 12-chem^{hi} EHL also featured increased expression of *IGHA* and this regulatory mechanism may thus be involved in the immune evasion of a subset of EHL. This overexpression of *IGHA* may suggest that isotype switching occurs in intra-EHL B cells and may appear contradictory with their immature phenotype. The IgA producing cells may however be generated outside of the liver, and, in this line, elevated numbers of IgA^{+} cells were identified in the spleen of the NASH murine models (30).

Our results are also in-line with the recent study by Moeini and colleagues who reported the inflammatory background of cirrhotic liver showing that patients with liver tissue exhibiting an immunosuppressive gene expression profile have a higher risk to develop malignant HCC (31). Additional studies will be needed to determine whether this signature impacts the immune changes that occur in dysplastic lesions.

In conclusion, our study demonstrates that a significant subset of EHL displays immature TLS formation and immune activation, along with overexpression of cytokines reported to be procarcinogenic in mice. This immune response appears inefficient to prevent progression to full-blown HCC and the expression of various immune checkpoint molecules in this subgroup of lesions may favor immune evasion. These results have implications for the development of anti-HCC chemopreventive strategies in cirrhotic patients, as fostering their antitumor immunity may limit the development of preneoplastic lesions.

Disclosure of Potential Conflicts of Interest

J.-M. Pawlotsky is an employee/paid consultant for AbbVie, Gilead, Merck, Siemens Healthcare, and GlaxoSmithKline. W.H. Fridman is an employee/paid consultant for AstraZeneca, Adaptimmune, Novartis, Catalym, Anaveon, and Ipsen, reports receiving commercial research grants from AstraZeneca, and holds ownership interest (including patents) in OSE Immunotherapeutics and HalioDX. No potential conflicts of interest were disclosed by the other authors.

Authors' Contributions

Conception and design: C. Sautes-Fridman, W.H. Fridman, J. Calderaro
Development of methodology: L. Lacroix, J. Calderaro
Acquisition of data (provided animals, acquired and managed patients, provided facilities, etc.): M. Meylan, F. Petitprez, L. Lacroix, L. Di Tommaso, M. Roncalli, A. Laurent, J. Derman, C. Charpy, J. Calderaro, D. Sommacale
Analysis and interpretation of data (e.g., statistical analysis, biostatistics, computational analysis): M. Meylan, F. Petitprez, J.-M. Pawlotsky, C. Sautes-Fridman, W.H. Fridman, J. Calderaro
Writing, review, and/or revision of the manuscript: M. Meylan, F. Petitprez, L. Di Tommaso, A. Laurent, G. Amaddeo, H. Regnault, F. Lafdil, J.-M. Pawlotsky, C. Sautes-Fridman, W.H. Fridman, J. Calderaro, D. Sommacale
Administrative, technical, or material support (i.e., reporting or organizing data, constructing databases): A. Bougoüin, G. Amaddeo
Study supervision: W.H. Fridman, J. Calderaro

Acknowledgments

Acknowledgments Authors warmly thank David Gentien, Emilie Henry, Audrey Rapinat, Laure Villoing-Gaude, and "Plateforme Génomique" of the Institut Curie (Paris, France) for performing NanoString analysis. The study was supported by Cancéropôle Ile-de-France (Emergence 2016), Fondation ARC (Aides individuelles), INCa (MUTHEC and HTE programs), Cancer Research for Personalized Medecine programme (CARPEM T8), Labex Immuno-Oncology (LAXE62_9UMRS972 FRIDMAN), Institut National de la Santé et de la Recherche Médicale, Université de Paris, Université Pierre et Marie Curie, and Programme Cartes d'Identité des Tumeurs (CIT) from the Ligue Nationale Contre le Cancer.

The costs of publication of this article were defrayed in part by the payment of page charges. This article must therefore be hereby marked *advertisement* in accordance with 18 U.S.C. Section 1734 solely to indicate this fact.

Received September 7, 2019; revised January 24, 2020; accepted April 3, 2020; published first April 8, 2020.

Downloaded from http://aacrjournals.org/clincancerres/article-pdf/26/16/4381/2062504/4381.pdf by guest on 27 August 2022

References

1. Llovet JM, Zucman-Rossi J, Pikarsky E, Sangro B, Schwartz M, Sherman M, et al. Hepatocellular carcinoma. Nat Rev Dis Primers 2016;2:16018.
2. Di Tommaso L, Franchi G, Park YN, Fiamengo B, Destro A, Morenghi E, et al. Diagnostic value of HSP70, glypican 3, and glutamine synthetase in hepatocellular nodules in cirrhosis. Hepatology 2007;45:725–34.
3. Nault JC, Calderaro J, Di Tommaso L, Balabaud C, Zafrani ES, Bioulac-Sage P, et al. Telomerase reverse transcriptase promoter mutation is an early somatic genetic alteration in the transformation of premalignant nodules in hepatocellular carcinoma on cirrhosis. Hepatology 2014;60:1983–92.
4. International Consensus Group for Hepatocellular Neoplasia. Pathologic diagnosis of early hepatocellular carcinoma: a report of the international consensus group for hepatocellular neoplasia. Hepatology 2009;49:658–64.
5. Rudini N, Novello C, Destro A, Riboldi E, Donadon M, Vigano L, et al. Phenotypic and molecular changes in nodule-in-nodule hepatocellular carcinoma with pathogenetic implications. Histopathology 2018;73:601–11.
6. Sciarra A, Di Tommaso L, Nakano M, Destro A, Torzilli G, Donadon M, et al. Morphophenotypic changes in human multistep hepatocarcinogenesis with translational implications. J Hepatol 2016;64:87–93.
7. Finkin S, Yuan D, Stein I, Taniguchi K, Weber A, Unger K, et al. Ectopic lymphoid structures function as microniches for tumor progenitor cells in hepatocellular carcinoma. Nat Immunol 2015;16:1235–44.
8. Nakagawa H, Umemura A, Taniguchi K, Font-Burgada J, Dhar D, Ogata H, et al. ER stress cooperates with hypernutrition to trigger TNF-dependent spontaneous HCC development. Cancer Cell 2014;26:331–43.
9. He G, Dhar D, Nakagawa H, Font-Burgada J, Ogata H, Jiang Y, et al. Identification of liver cancer progenitors whose malignant progression depends on autocrine IL-6 signaling. Cell 2013;155:384–96.
10. He G, Karin M.NF-κB and STAT3 - key players in liver inflammation and cancer. Cell Res 2011;21:159–68.
11. Galun E. Liver inflammation and cancer: the role of tissue microenvironment in generating the tumor-promoting niche (TPN) in the development of hepatocellular carcinoma. Hepatology 2016;63:354–6.
12. Pikarsky E, Porat RM, Stein I, Abramovitch R, Amit S, Kasem S, et al. NF-kappaB functions as a tumour promoter in inflammation-associated cancer. Nature 2004;431:461–6.
13. Greten FR, Eckmann L, Greten TF, Park JM, Li ZW, Egan LJ, et al. IKKbeta links inflammation and tumorigenesis in a mouse model of colitis-associated cancer. Cell 2004;118:285–96.
14. Sautes-Fridman C, Petitprez F, Calderaro J, Fridman WH. Tertiary lymphoid structures in the era of cancer immunotherapy. Nat Rev Cancer 2019;19:307–25.
15. Silina K, Soltermann A, Attar FM, Casanova R, Uckeley ZM, Thut H, et al. Germinal centers determine the prognostic relevance of tertiary lymphoid structures and are impaired by corticosteroids in lung squamous cell carcinoma. Cancer Res 2018;78:1308–20.
16. Posch F, Silina K, Leibl S, Mundlein A, Moch H, Siebenhuner A, et al. Maturation of tertiary lymphoid structures and recurrence of stage II and III colorectal cancer. Oncoimmunology 2018;7:e1378844.
17. Calderaro J, Petitprez F, Becht E, Laurent A, Hirsch TZ, Rousseau B, et al. Intratumoral tertiary lymphoid structures are associated with a low risk of early recurrence of hepatocellular carcinoma. J Hepatol 2018;70:58–65.
18. Ziol M, Pote N, Amaddeo G, Laurent A, Nault JC, Oberti F, et al. Macrotrabecular-massive hepatocellular carcinoma: a distinctive histological subtype with clinical relevance. Hepatology 2018;68:103–12.
19. Calderaro J, Couchy G, Imbeaud S, Amaddeo G, Letouze E, Blanc JF, et al. Histological subtypes of hepatocellular carcinoma are related to gene mutations and molecular tumour classification. J Hepatol 2017;67:727–38.
20. Calderaro J, Ziol M, Paradis V, Zucman-Rossi J. Molecular and histological correlations in liver cancer. J Hepatol 2019;71:616–30.
21. Murakami J, Shimizu Y, Kashii Y, Kato T, Minemura M, Okada K, et al. Functional B-cell response in intrahepatic lymphoid follicles in chronic hepatitis C. Hepatology 1999;30:143–50.
22. Wickham H. Ggplot2 elegant graphics for data analysis. New York, NY: Springer; 2009.
23. Coppola D, Nebozhyn M, Khalil F, Dai H, Yeatman T, Loboda A, et al. Unique ectopic lymph node-like structures present in human primary colorectal carcinoma are identified by immune gene array profiling. Am J Pathol 2011;179:37–45.
24. Messina JL, Fenstermacher DA, Eschrich S, Qu X, Berglund AE, Lloyd MC, et al. 12-Chemokine gene signature identifies lymph node-like structures in melanoma: potential for patient selection for immunotherapy? Sci Rep 2012;2:765.
25. Sia D, Jiao Y, Martinez-Quetglas I, Kuchuk O, Villacorta-Martin C, Castro de Moura M, et al. Identification of an immune-specific class of hepatocellular carcinoma, Based on Molecular Features. Gastroenterology 2017;153:812–26.
26. Kurebayashi Y, Ojima H, Tsujikawa H, Kubota N, Maehara J, Abe Y, et al. Landscape of immune microenvironment in hepatocellular carcinoma and its additional impact on histological and molecular classification. Hepatology 2018;68:1025–41.
27. Calderaro J, Rousseau B, Amaddeo G, Mercey M, Charpy C, Costentin C, et al. Programmed death ligand 1 expression in hepatocellular carcinoma: relationship with clinical and pathological features. Hepatology 2016;64:2038–46.
28. Latchman Y, Wood CR, Chernova T, Chaudhary D, Borde M, Chernova I, et al. PD-L2 is a second ligand for PD-1 and inhibits T cell activation. Nat Immunol 2001;2:261–8.
29. Haybaeck J, Zeller N, Wolf MJ, Weber A, Wagner U, Kurrer MO, et al. A lymphotoxin-driven pathway to hepatocellular carcinoma. Cancer Cell 2009;16:295–308.
30. Shalapour S, Lin XJ, Bastian IN, Brain J, Burt AD, Aksenov AA, et al. Inflammation-induced IgA+ cells dismantle anti-liver cancer immunity. Nature 2017;551:340–5.
31. Moeini A, Torrecilla S, Tovar V, Montironi C, Andreu-Oller C, Peix J, et al. An immune gene expression signature associated with development of human hepatocellular carcinoma identifies mice that respond to chemopreventive agents. Gastroenterology 2019;157:1383–97.

Downloaded from http://aacrjournals.org/clincancerres/article-pdf/26/16/4381/2062504/4381.pdf by guest on 27 August 2022